Effect of interference of crack faces on shear-mode threshold for small fatigue cracks in a bearing steel

H. Matsunaga[1]

[1] Department of Mechanical Engineering, Fukuoka University, 8-19-1 Nanakuma, Jonan-ku, Fukuoka, 814-0180, Japan, hm@fukuoka-u.ac.jp

ABSTRACT. *The near-threshold fatigue behavior of small, semi-elliptical surface cracks in a martensitic bearing steel was investigated under cyclic shear-mode loading in ambient air. Various sizes of artificial defects were introduced onto cylindrical specimens as a crack starter. Fully-reversed torsion was combined with a static axial compression to obtain a stable shear-mode crack growth parallel to the specimen axis. The crack growth curves were stepwise, i.e. stop-and-go growth processes were repeated during the test. These cracks took a very large number of cycles to grow, and the crack growth rate, da/dN, was ranged from 10^{-13} to 10^{-10} m/cycle. The torsional stress was gradually decreased with an increase in crack length and finally the cracks became non-propagating. The mode II threshold stress intensity factor ranges, ΔK_{IIth}, was significantly dependent on not only on crack sizes but also on interference between crack faces.*

INTRODUCTION

Shear-mode crack has been a major concern for researchers studying rolling-contact fatigue failures, such as the flaking in bearings and the shelling in rails [1-3]. In order to deal with these problems as a crack problem, the crack behavior should be determined. Although there has been significant progress in recent years [1-3], shear-mode growth is still not well understood, neither qualitatively nor from a quantitative fracture mechanics point of view, especially in hard steels.

In this study, near-threshold behavior of semi-elliptical shear-mode fatigue cracks less than 1 mm in size were studied in cylindrical specimens of SAE52100 bearing steel in ambient air. Critical experiments involving the growth of small shear-mode cracks were carried out to determine the role of crack-face interference and the crack size dependency on the threshold value.

EXPERIMENTAL

Tested Material

The studies were carried out using a commercial grade SAE52100 bearing steel. The

chemical composition in mass % is 1.01 C, 0.26 Si, 0.37 Mn, 0.011 P, 0.006 S, 0.06 Cu, 0.06 Ni, 1.45 Cr, 0.03 Mo and bal. Fe. The steel was heat-treated at 840°C for 30 minutes in a deoxidizing gas followed by oil-quenching and tempering at 170°C for 2 hours. The average Vickers hardness *HV* measured with a load of 9.8 N was 753.

Specimens and Artificial Defects

Figure 1 shows the shape and dimensions of fatigue specimens. The specimen surfaces were finished by polishing with an emery paper and then by buffing with an alumina paste. The following two types of artificial defects with various sizes were introduced; (i) three adjacent, shallow drilled holes which have crack-like thin slits made by the focused ion beam (FIB) technique at the both ends, and (ii) a semi-circular slit made by the electrical discharging and which also has the FIB slits at both ends. The processes of both FIB and electrical discharging did not induce any degradation of material, such as the decrease in hardness, within the region that is involved in the determination of crack growth threshold. Figure 2 shows the shape and dimensions of these defects, which are designated as Type A ~ E, respectively. All of these defects were aligned parallel to the specimen axis.

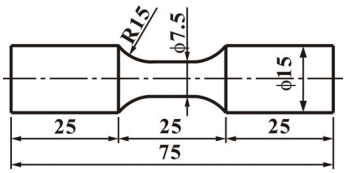

Figure 1. Shape and dimensions of round test specimen, in mm.

Fatigue Tests

Fully reversed cyclic torsion tests were carried out using a tension-torsion servo-hydraulic fatigue testing machine which was operated at a test frequency of 10 ~ 28 Hz in ambient air. In an effort to suppress the tendency for mode I crack branching, an axial static compressive stress σ_s of −1200 MPa was superposed on the torsional cyclic load. Since, with minor variations, the cracks grew parallel to the specimen axis in all of the tests, there are neither any singular stresses associated with opening mode SIF, K_I, nor compressive stress acting normal to the crack face during testing. The tests were periodically halted for microscopic observation of the crack initiation and crack growth processes.

RESULTS AND DISCUSSION

Crack Growth Behaviors and Threshold Stresses

Due to the combination of static axial compression with cyclic torsion, cracks were propagated parallel to the specimen axis without branching in mode I directions.

To determine threshold stress for the shear-mode cracks of various sizes, after every 5 ~ 40 μm increment in crack length $2a$, torsional stress amplitude, τ_a, was decreased in steps of 5 ~ 40 MPa from the initial value. Figure 3 shows examples of crack growth curves for specimens having Types A and B defects. The crack growth curves were stepwise, *i.e.* stop-and-go growth processes were repeated during the test. Figure 4 shows

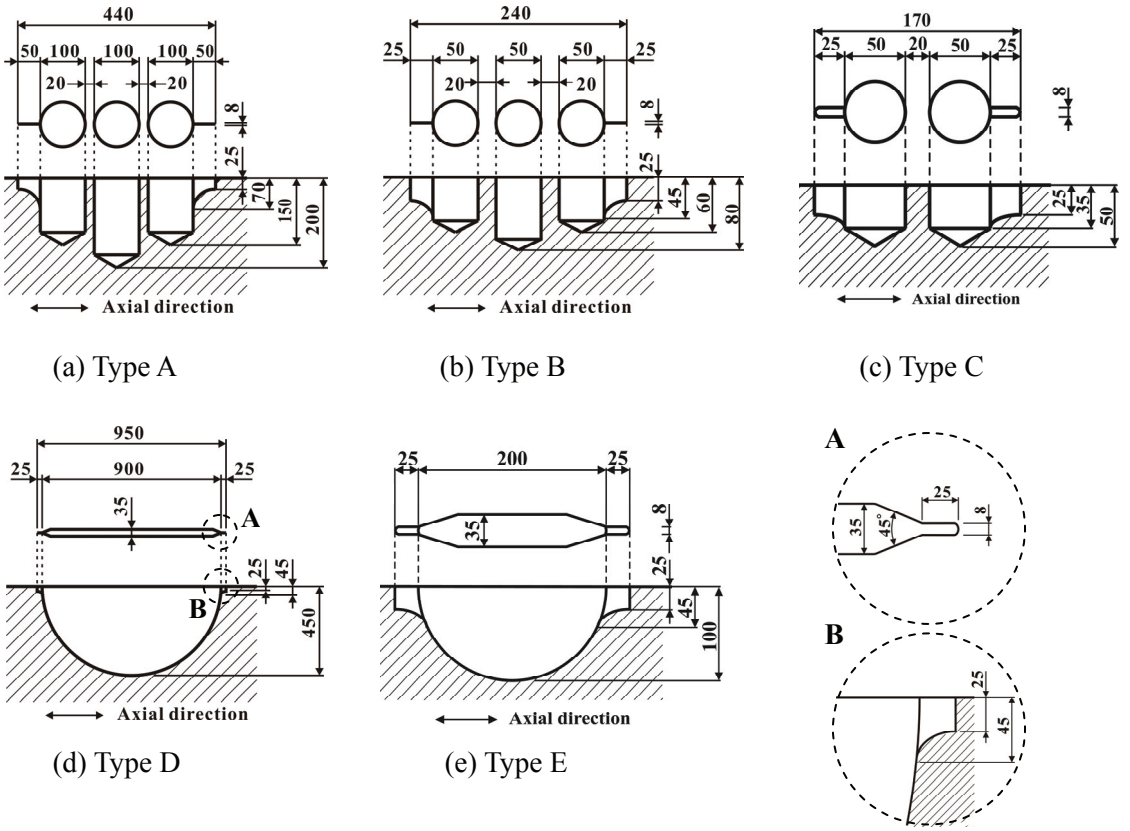

(a) Type A (b) Type B (c) Type C

(d) Type D (e) Type E

(f) Detail of regions A and B in (d)

Figure 2. Shapes and dimensions of defects having crack-like thin slits at the both ends, in μm.

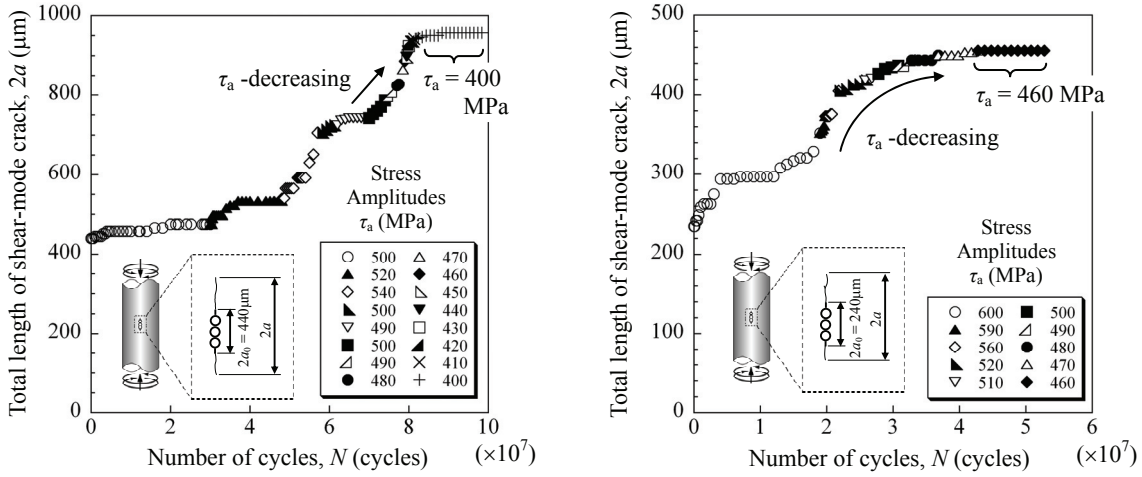

(a) Crack growth from Type A defect (b) Crack growth from Type B defect

Figure 3. Crack growth curves.

the crack growth rate, da/dN, as a function of ΔK_{II} in the vicinity of specimen surface. The ΔK_{II} was calculated by assuming that the aspect ratio of propagating crack was equivalent to that of non-propagating crack. The details of calculation of ΔK_{II} will be explained in the next section. These cracks took a very large number of cycles to grow, and crack growth rate, da/dN, was ranged from 10^{-13} to 10^{-10} m/cycle. When a crack did not propagate during an additional 10^7 cycles after a decrease in τ_a, the crack was considered to be a non-propagating crack, and the corresponding stress amplitude was considered to be the threshold stress. Figure 5 shows the non-propagating cracks.

Shapes of Non-prpagating Cracks and ΔK_{IIth}

Figure 6 shows the shapes and dimensions of the non-propagating cracks shown in Fig. 6, which were obtained by a successive polishing of the specimen surfaces after the non-propagating stage had been reached. Mode I branching was not observed along the crack fronts of these cracks, hence it was considered that these cracks had propagated in a pure shear-mode.

The mode II threshold SIF ranges, ΔK_{IIth}, were estimated from the dimensions of non-propagating cracks. In a shear-mode semi-elliptical crack, such as the cracks in Fig. 6, crack propagates in mode III at the crack depth, whereas in the vicinity of free surface the propagation is dominated by mode II. In this study, the ΔK_{II} were approximated with Kassir and Sih's solution [4] for an elliptical crack in an infinite body under uniform shear. It is noted that the solution provides good agreement with the SIFs for semi-elliptical cracks except in the vicinity of corner point. The obtained values of ΔK_{IIth} are shown in the captions of Fig.5 and Fig.6.

Effect of Interference of Crack Faces on Threshold Value

A microstructural change was observed over the crack faces, as the author *et al.* reported previously [5]. It is also noted that the debris which was a product of the abrasion process continued to emerge from cracks during fatigue tests [5]. The changed microstructure

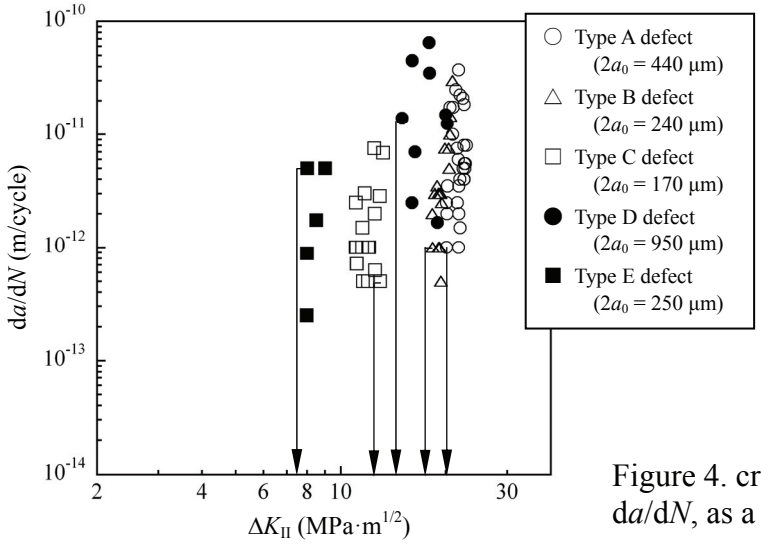

Figure 4. crack growth rate, da/dN, as a function of ΔK_{II}.

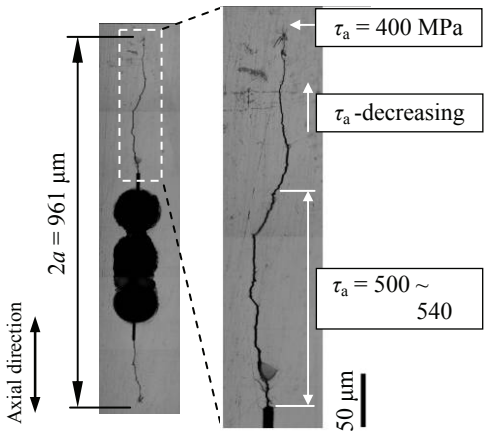

(a) Type A defect (τ_a = 540 MPa → 400 MPa, σ_s = –1200 MPa, N_{total} = 9.84×10^7, ΔK_{IIth}=20.3 MPa·m$^{1/2}$, f=79.5 %)

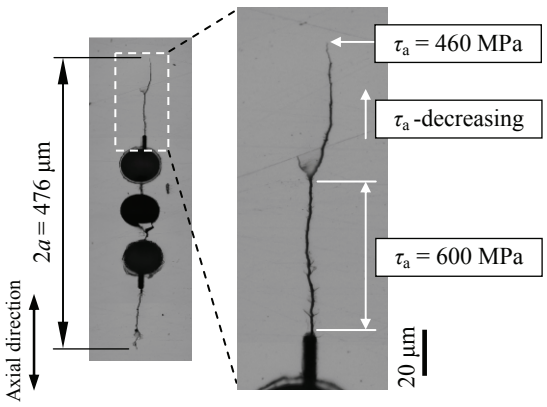

(b) Type B defect (τ_a = 600 MPa → 460 MPa, σ_s = –1200 MPa, N_{total} = 5.28×10^7, ΔK_{IIth}=17.9 MPa·m$^{1/2}$, f=84.8 %)

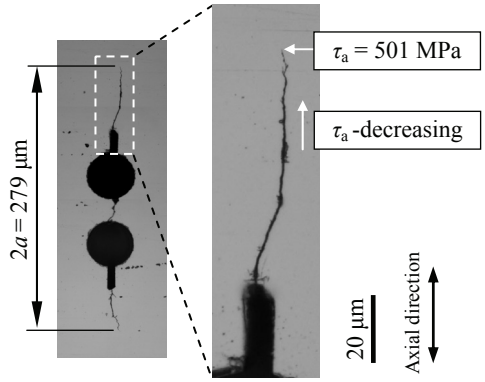

(c) Type C defect (τ_a = 521 MPa → 501 MPa, σ_s = –1200 MPa, N_{total} = 7.78×10^7, ΔK_{IIth}=12.4 MPa·m$^{1/2}$, f =66.8 %)

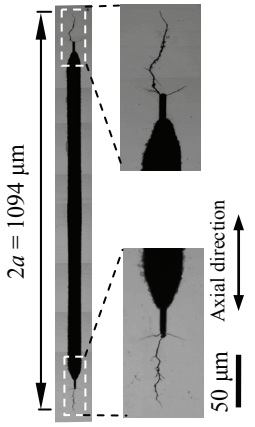

(d) Type D defect (τ_a = 355 MPa → 243 MPa, σ_s = –1200 MPa, N_{total} = 1.85×10^7, ΔK_{IIth}=14.0 MPa·m$^{1/2}$, f=4.0 %)

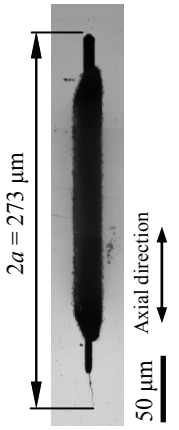

(e) Type E defect (τ_a = 332 MPa → 275 MPa, σ_s = –1200 MPa, N_{total} = 2.65×10^7, ΔK_{IIth}=7.5 MPa·m$^{1/2}$, f=8.1 %)

Figure 5 Non-propagating cracks (Optical microscope).

and the production of debris both indicated that crack growth threshold had been increased by the interference of crack faces due to the mechanical interlocking of asperities. Such a reduction of effective stress at crack tip has been studied by many researchers [1-3, 6] and termed, for example, “sliding mode crack closure” [6].

In order to quantify how much the crack-face interference increased the threshold value, a correlation between ΔK_{IIth} and area of interfering crack face was examined. The values of ΔK_{IIth} for the various interfering area were compared at about the same crack sizes since there is a crack size dependency on ΔK_{IIth}, which will be discussed in the next

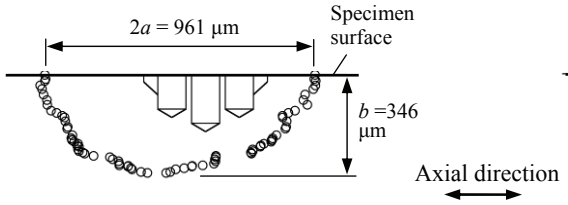

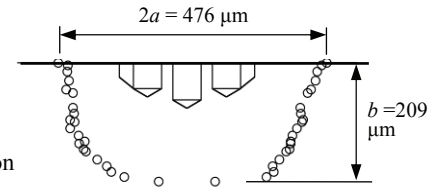

Axial direction

(a) Crack shown in Fig. 5(a) (Type A defect, τ_a-decreasing, τ_a = 540 MPa → 400 MPa, σ_s = –1200 MPa, N_{total} = 9.84×10^7, ΔK_{IIth}=20.3 MPa·m$^{1/2}$, f=79.5 %)

(b) Crack shown in Fig. 5(b) (Type B defect, τ_a-decreasing, τ_a = 600 MPa → 460 MPa, σ_s = –1200 MPa, N_{total} = 5.28×10^7, ΔK_{IIth}=17.9 MPa·m$^{1/2}$, f=84.8 %)

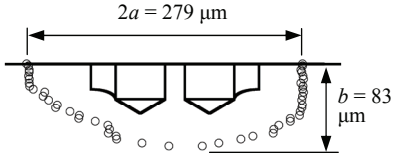

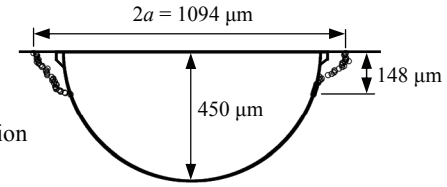

Axial direction

(c) Crack shown in Fig. 5(c) (Type C defect, τ_a-decreasing, τ_a = 521 MPa → 501 MPa, σ_s = –1200 MPa, N_{total} = 7.78×10^7, ΔK_{IIth}=12.4 MPa·m$^{1/2}$, f=66.8 %)

(d) Crack shown in Fig. 5(d) (Type D defect, τ_a-decreasing, τ_a = 355 MPa → 243 MPa, σ_s = –1200 MPa, N_{total} = 1.85×10^7, ΔK_{IIth}=14.0 MPa·m$^{1/2}$, f=4.0 %)

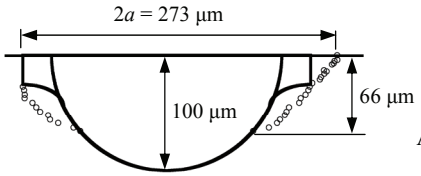

Axial direction

(e) Crack shown in Fig. 5(e) (Type E defect, τ_a-decreasing, τ_a = 332 MPa → 275 MPa, σ_s = –1200 MPa, N_{total} = 2.65×10^7, ΔK_{IIth}=7.5 MPa·m$^{1/2}$, f=8.1 %)

Figure 6. Shapes and dimensions of non-propagating cracks obtained by successive polishing.

section. Figure 7 shows ΔK_{IIth} for two crack sizes, 2a of ≈ 1 mm and ≈ 0.28 mm, as a function of the fraction of interfering crack area f, which was defined by the area of interfering crack face divided by the total area of defect plus crack. The definition of f is shown also in Fig. 7. The values of f are also shown in the captions of Fig. 5 and Fig. 6. The ΔK_{IIth} decreased with a decrease in f for both crack sizes. This means that the sliding mode crack closure played a major role in determining the crack growth threshold. The value of ΔK_{IIth} extrapolated to f = 0 % in Fig. 7 is considered to be the threshold value in the absence of sliding mode crack closure. Supposing the ΔK_{IIth} to be a linear function of f, ΔK_{IIth} for f = 0 % was estimated to be 13 MPa·m$^{1/2}$ for 2a ≈ 1 mm, and 6.8 MPa·m$^{1/2}$ for 2a ≈ 0.28 mm. On the other hand, the ΔK_{IIth} extrapolated to f = 100 %, was 22 MPa·m$^{1/2}$ for 2a ≈ 1 mm, and 15 MPa·m$^{1/2}$ for 2a ≈ 0.28 mm.

Crack Size Dependency on Threshold Value

Figure 8 shows all the threshold values obtained in this study as a function of crack size. In Fig. 8, additional data of ΔK_{IIth} and $\Delta K_{\mathrm{IIIth}}$ were also plotted, which were obtained in the author *et al.*'s previous study. ΔK_{IIth} was plotted for the half crack length a, and $\Delta K_{\mathrm{IIIth}}$ for the crack depth b, respectively. Number adjacent to each plot indicates the fraction of interfering crack area, f. The two broken lines show the ΔK_{IIth} for $f = 0$ % and $f = 100$ % obtained from the extrapolation in Fig. 7. All the data with various f appear to distribute between these lines. The threshold values decreased with a decrease in crack size where a or b is less than 1 mm regardless of the presence of crack-face interference. Such a dependency on the threshold value is well known in the case of mode I cracks. [7, 8] Also with respect to mode III cracks, Toyama *et al.* [9] and Beretta *et al.* [10] have reported the crack size dependency on fatigue crack growth in a medium carbon steel and a gear steel. Note that this crack size effect can become of importance also in estimating the rolling contact fatigue strength from the fracture mechanics point of view since the value for a large crack gives an unconservative estimation.

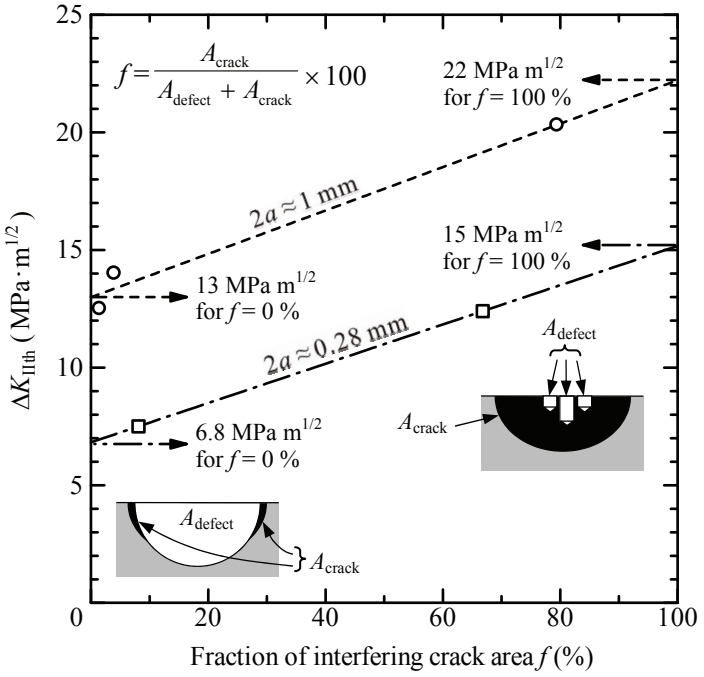

Figure 7. ΔK_{IIth} for 1 mm-long and 0.28 mm-long cracks as a function of fraction of interfering crack area to the total area of defect plus crack, f.

CONCLUSIONS

The following conclusions were obtained.

(1) Threshold stress intensity factor ranges, ΔK_{IIth}, decreased with a decrease in crack size. In estimating the rolling contact fatigue strength as a crack problem, the crack size effect cannot be ignored.

(2) An interference of crack faces raised the threshold value even though there was no

compressive stress normal to crack face. The ΔK_{IIth} in the absence of interference of crack faces was estimated to be 13 MPa·m$^{1/2}$ for a 1 mm-long crack and 6.8 MPa·m$^{1/2}$ for a 0.28 mm-long crack.

REFERENCES

1. Murakami, Y., Fukushima, Y., Toyama, K. and Matsuoka, S. (2008) *Engineering Fracture Mechanics* **75**, 306-318.
2. Otsuka, A., Fujii, Y. and Maeda, K. (2004) *Fatigue Fract. Engng Mater. Struct.* **27**, 203-212.
3. Murakami, Y., Fukuhara, T. and Hamada, S. (2002) *Journal of the Society of Materials Science, Japan* **51**, 918-925.
4. Kassir, M.K. and Sih, G.C. (1966) *Journal of Applied Mechanics* **33**, 601-611.
5. Matsunaga, H., Muramoto, S., Shomura, N. and Endo, M. (2009) *Journal of the Society of Materials Science, Japan* **58**, 773-780.
6. Tschegg, E.K. (1983) *Acta Metall.* **31**, 1323-1330.
7. Kitagawa, H. and Takahashi, S. (1979) *Transactions of the Japan Society of Mechanical Engineers* **A45**, 1289-1303.
8. Murakami, Y. (2002). In: *Metal Fatigue: Effects of Small Defects and Nonmetallic Inclusions*, Elsevier Ltd., Oxford, UK.
9. Toyama, K., Takahashi, K. and Murakami, Y. (2003) *Proc. International Conference on Advanced Technology in Experimental Mechanics 2003 (ATEM'03)*, CD-ROM.
10. Beretta, S., Foletti, S. and Valiullin, K. (2009) *Proc. International Conference on Crack Paths (CP 2009)*, 48-59.

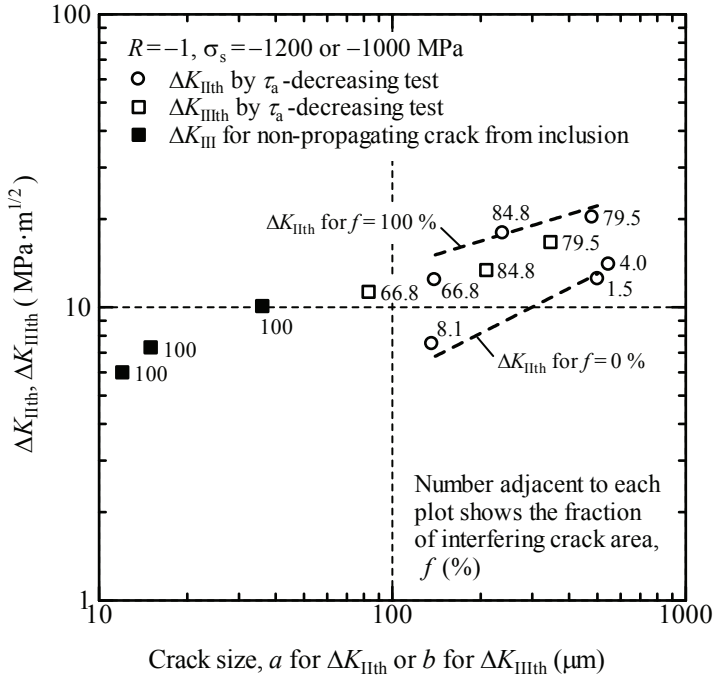

Figure 8. Relationship between crack sizes and crack-growth thresholds.